Enhancement of the Upper Critical Field in Disordered Transition Metal Dichalcogenide Monolayers

Stefan Ilić, Julia S. Meyer, and Manuel Houzet
Univ. Grenoble Alpes, CEA, INAC-PHELIQS, F-38000 Grenoble, France
(Received 4 May 2017; published 11 September 2017)

We calculate the effect of impurities on the superconducting phase diagram of transition metal dichalcogenide monolayers in the presence of an in-plane magnetic field. Because of strong intrinsic spin-orbit coupling, the upper critical field greatly surpasses the Pauli limit at low temperatures. We find that it is insensitive to intravalley scattering and, ultimately, limited by intervalley scattering.

DOI: 10.1103/PhysRevLett.119.117001

Introduction.—Transition metal dichalcogenide (TMDC) monolayers are recently discovered as two-dimensional (2D) semiconductors of the form MX_2 (M = Mo, Nb, or W, and X = S, Se, or Te), with a hexagonal lattice structure similar to graphene, but with two inequivalent sites in the unit cell [1,2]. Like graphene, these materials exhibit a valley degree of freedom and have minima (maxima) of conduction (valence) bands at the corners $\mathbf{K}$ and $-\mathbf{K}$ of the Brillouin zone [3]. Unlike graphene, however, the absence of inversion symmetry allows for a large, direct band gap, making them promising candidates for a new generation of transistors [1,4].

Because of the heavy constituent atoms, TMDC monolayers exhibit a very large intrinsic spin-orbit coupling (SOC), often called Ising SOC [5], which acts as an effective Zeeman field perpendicular to the plane of the material with opposite orientations in the two valleys [6–8]. As a consequence, a large valley-dependent spin-splitting occurs in the valence band as well as in the conduction band, though with a much smaller magnitude (due to the predominant $d_{x^2-y^2} \pm id_{xy}$ and d_{z^2} orbital character of carriers, respectively). Recent optical investigations have confirmed that electrons from different valleys can be excited selectively with circularly polarized light [9,10]. These properties open the door for novel applications in spintronics and so-called valleytronics [8,11].

The coupling between the spin and valley degrees of freedom has remarkable repercussions for the superconducting properties that have been reported in these materials. In heavily n-doped ionic-gated MoS_2 flakes, a 2D superconducting phase with a critical temperature T_c around 10 K has been observed [12,13]. Interestingly, the in-plane upper critical field H_{c2} reaches up to 60 T, thus greatly surpassing the Pauli limit, $H_P = \sqrt{2}\Delta_0/(g\mu_B)$, where $\Delta_0 \simeq 1.76 k_B T_c$, μ_B is the Bohr magneton, and g the g factor. This is interpreted as a consequence of the interplay of Ising SOC and the 2D nature of the materials. Namely, in 2D materials the orbital pair-breaking effect is largely suppressed for an in-plane magnetic field [14]. On the other hand, due to the Ising SOC, the in-plane magnetic field is also not efficient for breaking Cooper pairs by the paramagnetic effect, as they are formed of electrons in opposite valleys with strongly pinned out-of-plane spins. Related results have also been reported in superconducting $NbSe_2$ monolayers in the p-doped regime [15]. Existing theories only considered the clean case [12,16] and do not describe all the experimental observations.

In this work, we establish the theory of the upper critical field for Ising superconductors at arbitrary disorder strength, assuming a conventional s-wave Cooper pairing. The enhancement of the in-plane upper critical field above the Pauli limit is a general feature of superconductivity in the presence of SOC. It has been predicted in disordered 2D superconductors with spin-orbit scattering [17,18] or Rashba SOC [19]. The latter has been invoked to interpret recent experiments on oxide interfaces [20] and Pb monolayer films [21]. Ising SOC leads to qualitatively different effects. Using a simple model, we show that Ising superconductivity results in a much larger enhancement and exhibits several new and interesting properties. Namely, H_{c2} diverges at low temperature—a phenomenon which is robust to intravalley scattering. On the other hand, intervalley scattering provides an effective spin-flip scattering mechanism and leads to the saturation of H_{c2}, consistent with the experimental findings. Furthermore, we show that, in contrast with Rashba SOC [22], Ising SOC does not stabilize a spatially nonuniform superconducting phase.

Understanding the role of impurities is important for future applications of TMDCs and their incorporation into van der Waals heterostructures [23]. The doping techniques used to prepare the superconducting samples, as well as the defects in the crystal lattice could be the source of significant disorder. Recent weak localization measurements in MoS_2 monolayers suggest substantial intervalley scattering, attributed to a high concentration of sulfur vacancies in the monolayer [24]. Our result will contribute to identifying the superconducting properties of these materials in the presence of disorder and assess their potential for applications such as in superconducting spintronics.

The model.—The Hamiltonian describing the normal state of TMDC monolayers in the vicinity of the $\pm\mathbf{K}$ points in the presence of a parallel magnetic field is [7] (we use units, where $\hbar = k_B = 1$)

$$\mathcal{H}_{\mathbf{q}} = v(q_x\sigma_x\eta_z + q_y\sigma_y) + E_g\sigma_z + [\Delta_A(\sigma_z+1) + \Delta_B(\sigma_z-1)]s_z\eta_z + hs_x. \quad (1)$$

Here, $\mathbf{q} = (q_x, q_y)$ is a small momentum measured from $\pm\mathbf{K}$, v is the velocity associated with the linearized kinetic dispersion, E_g is the difference in on-site energy responsible for the opening of a band gap, and Δ_A and Δ_B are spin-splitting parameters on two different sublattices. Furthermore, $\sigma_{x,y,z}$, $s_{x,y,z}$, and $\eta_{x,y,z}$ are Pauli matrices acting in sublattice, spin, and valley spaces, respectively, and the Zeeman energy $h = \frac{1}{2}g\mu_B B$ is related with the amplitude of the magnetic field and the in-plane g factor.

We proceed by projecting the Hamiltonian (1) to the conduction band (n-doped regime). The spin-independent part of the Hamiltonian (1) gives the dominant contribution to the energy of the system and has a simple spectrum $\xi_{\mathbf{q}} = \sqrt{v^2|\mathbf{q}|^2 + E_g^2}$. It is diagonalized by the unitary transformation $U_{\mathbf{q}} = \exp[i\alpha_{\mathbf{q}}\sigma_y\eta_z]\exp[i\beta_{\mathbf{q}}\sigma_z\eta_z]$, with $\tan(2\alpha_{\mathbf{q}}) = v|\mathbf{q}|/E_g$ and $\tan(2\beta_{\mathbf{q}}) = q_y/q_x$. By assuming $\xi_{\mathbf{q}} \gg \Delta_A, \Delta_B$ and by projecting $U_{\mathbf{q}}\mathcal{H}_{\mathbf{q}}U_{\mathbf{q}}^\dagger$ onto the conduction band, we obtain

$$\mathcal{H}_{\eta\mathbf{q}} = \xi_{\mathbf{q}} + \eta\Delta_{so}(\mathbf{q})s_z + hs_x, \quad (2)$$

where $\eta = \pm 1$ represents the valley index and $\Delta_{so}(\mathbf{q}) = 1/2[\Delta_A - \Delta_B + (\Delta_A + \Delta_B)E_g/\xi_{\mathbf{q}}]$ is an effective SOC parameter [25]. A Hamiltonian similar to Eq. (2) with $\xi_{\mathbf{q}} \to -\xi_{\mathbf{q}}$ holds in the valence band (p-doped regime). Below, we will assume that the chemical potential μ is sufficiently far above E_g [26] on the relevant energy scales determining the superconducting properties ($h, \Delta, T, \ldots \ll |\mu - E_g|$), so that Δ_{so} can be taken as a constant. The energy spectrum of Hamiltonian (3) is illustrated in Fig. 1.

Superconductivity is described using a standard Bardeen-Cooper-Schrieffer (BCS) Hamiltonian, where the singlet pairing of electrons into Cooper pairs is necessarily intervalley. The corresponding mean-field Hamiltonian reads

$$H_{\mathrm{BCS}} = \sum_{\eta\mathbf{q}} c_{\eta\mathbf{q}}^\dagger \mathcal{H}_{\eta\mathbf{q}} c_{\eta\mathbf{q}} + \Delta\sum_{\eta\mathbf{q}} c_{\eta\mathbf{q}\uparrow}^\dagger c_{\bar{\eta}\,\bar{\mathbf{q}}\downarrow}^\dagger + \mathrm{H.c.}, \quad (3)$$

where $c_{\eta\mathbf{q}} = (c_{\eta\mathbf{q}\uparrow}, c_{\eta\mathbf{q}\downarrow})^T$ is an annihilation operator for spin-up and spin-down electrons, and Δ is the superconducting order parameter. For compactness, we use the abbreviations $\bar{\eta} = -\eta$ and $\bar{\mathbf{q}} = -\mathbf{q}$. In the vicinity of the second-order superconducting phase transition, Δ solves the linearized self-consistent gap equation

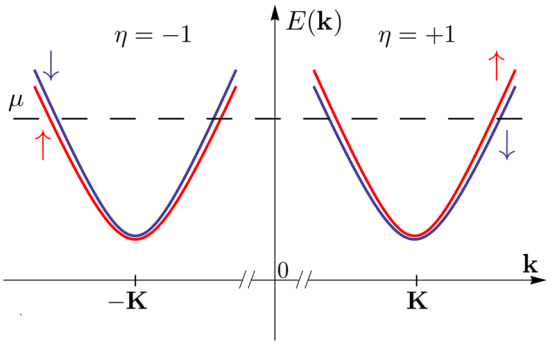

FIG. 1. Schematic representation of the conduction band of TMDC monolayers in the vicinity of the corners of the Brillouin zone as described by Eq. (2). The spin splitting in the two valleys is opposite due to the so-called Ising SOC.

$$\Delta = \frac{\lambda T}{4}\sum_{\eta,\mathbf{q},|\omega|<\Omega} \mathrm{Tr}[is_y\mathcal{G}^+_{\bar{\eta}\,\bar{\mathbf{q}}\,\omega}\Delta is_y\mathcal{G}^-_{\eta\mathbf{q}\omega}], \quad (4)$$

where λ is the BCS pairing amplitude and Ω is a cutoff frequency. The particle and hole Green's functions are given as $\mathcal{G}^-_{\eta\mathbf{q}\omega} = (i\omega - \mathcal{H}_{\eta\mathbf{q}})^{-1}$ and $\mathcal{G}^+_{\eta\mathbf{q}\omega} = (-i\omega - \mathcal{H}^T_{\eta\mathbf{q}})^{-1}$, respectively, with Matsubara frequencies $\omega = (2n+1)\pi T$, $n \in \mathbb{Z}$, at temperature T.

Scattering potential.—The effect of impurities in 2D hexagonal lattices was extensively studied in the case of graphene [28,29]. Here we study the dominant scattering terms, namely, spin-independent intra- and intervalley scattering, which may originate from long-range Coulomb interactions or defects in the lattice. Their contribution, expressed in the same basis as the normal state Hamiltonian (1), reads

$$\mathcal{H}_D(\mathbf{q}-\mathbf{q}') = V_1(\mathbf{q}-\mathbf{q}') + \sum_{i=x,y} V_{2i}(\mathbf{q}-\mathbf{q}')\eta_i. \quad (5)$$

The random disorder potentials are characterized by the Gaussian correlators $\langle V_\alpha(\mathbf{q})V_\beta(\bar{\mathbf{q}}')\rangle = w_\alpha^2\delta_{\alpha,\beta}\delta_{\mathbf{q},\mathbf{q}'}$, where $\alpha, \beta = 1, 2x, 2y$, and the brackets denote disorder averaging. The ratio $w_{2i}/w_1 \sim 1/(|\mathbf{K}|^2R^2)$, which is related with the range R of the potential created by a single impurity, is typically small for remote impurities and of order 1 for lattice defects.

Then, projecting the Hamiltonian $U_{\mathbf{q}}\mathcal{H}_D(\mathbf{q}-\mathbf{q}')U_{\mathbf{q}'}^\dagger$ onto the conduction band, we find that Eq. (3) has to be supplemented with the disorder term

$$H_D = \sum_{\eta\mathbf{q}\mathbf{q}'} \mathcal{V}_{1\mathbf{q}\mathbf{q}'}c_{\eta\mathbf{q}}^\dagger c_{\eta\mathbf{q}'} + \mathcal{V}_{2\mathbf{q}\mathbf{q}'}c_{\eta\mathbf{q}}^\dagger c_{\bar{\eta}\mathbf{q}'} + \mathrm{H.c.}, \quad (6)$$

where $\mathcal{V}_{1\mathbf{q}\mathbf{q}'} = V_1(\mathbf{q}-\mathbf{q}')\cos(\theta-\theta')/2$ and $\mathcal{V}_{2\mathbf{q}\mathbf{q}'} = [i\eta V_{2x}(\mathbf{q}-\mathbf{q}') - V_{2y}(\mathbf{q}-\mathbf{q}')]\sin(\theta+\theta')/2$ with $\mathbf{q}^{(\prime)} = |\mathbf{q}^{(\prime)}|(\cos\theta^{(\prime)}, \sin\theta^{(\prime)})$.

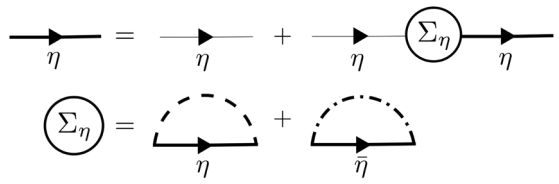

FIG. 2. Diagrammatic representation of the Dyson equation and the self-energy in the self-consistent Born approximation. The thin arrow represents the "bare", disorder-free Green's function $\mathcal{G}_\eta^\pm$, while the thick arrow is the disorder-averaged Green's function $\langle \mathcal{G}_\eta^\pm \rangle$. The dashed and dot-dashed impurity lines represent intra- and intervalley scattering events, respectively.

The disorder-averaged Green's function can be calculated from the Dyson equation represented diagrammatically in Fig. 2. That is, $\langle \mathcal{G}^\pm_{\eta\mathbf{q}\omega}\rangle = (\mathcal{G}^\pm_{\eta\mathbf{q}\omega}{}^{-1} - \Sigma^\pm_\eta)^{-1}$, where the self-energy $\Sigma^\pm_\eta$ is obtained using the self-consistent Born approximation. As a result, we find $\Sigma^\pm_\eta = \mp i[1/(2\tau_1) + 1/(2\tau_2)]\mathrm{sgn}(\omega)$, where $1/\tau_1 = \pi\nu w_1^2$ and $1/\tau_2 = \pi\nu(w_{2x}^2 + w_{2y}^2)$ are the intra- and intervalley elastic scattering rates, respectively, $\nu = \mu/(2\pi v_F^2)$ is the density of states per spin at the Fermi level, and v_F is the Fermi velocity.

Upper critical line.—The upper critical field $h_{c2}(T) = \frac{1}{2} g\mu_B H_{c2}(T)$ can be calculated from the disorder-averaged gap equation (4). This involves finding the averages of the products of two Green's functions, which we do in the standard ladder approximation, as shown in Fig. 3(a). The first diagram represents the bare vertex, while the second one is a ladder diagram, expressed in terms of eight vertex functions $\Pi_\eta^{ss'}$ (4 combinations of spin indices and 2 values of the valley index), which solve coupled Bethe-Salpeter equations; see Fig. 3(b). Solving these equations yields a remarkably simple expression [30]:

$$\ln\frac{T}{T_c} = 2\pi T \sum_{\omega>0}\left[\frac{\omega(\omega+\frac{1}{\tau_2}) + \Delta_{so}^2}{(\omega+\frac{1}{\tau_2})(\omega^2 + h_{c2}^2 + \Delta_{so}^2) - \frac{\Delta_{so}^2}{\tau_2}} - \frac{1}{\omega}\right], \qquad (7)$$

where we used the standard BCS result $T_c \simeq 1.13\Omega e^{-1/(\lambda\nu)}$. Note that Eq. (7) holds for arbitrary values of the intravalley scattering rate. Below we analyze this equation, which is the main result of this Letter.

Without intervalley scattering.—In the absence of intervalley scattering, $1/\tau_2 = 0$, the critical line given by Eq. (7) does not depend on disorder (Anderson theorem). In that case, Eq. (7) can be alternatively expressed as

$$\ln\frac{T_c}{T} = \frac{h_{c2}^2}{h_{c2}^2 + \Delta_{so}^2}\Re\left[\psi\left(\frac{1}{2} + \frac{i\sqrt{h_{c2}^2 + \Delta_{so}^2}}{2\pi T}\right) - \psi\left(\frac{1}{2}\right)\right], \qquad (8)$$

where $\psi(z)$ is the digamma function. In this form, it ressembles—and generalizes to arbitrary disorder—an

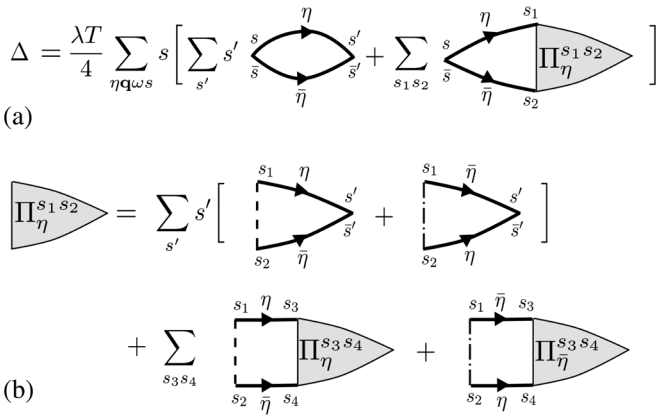

FIG. 3. (a) Diagrammatic representation of the disorder-averaged self-consistency condition given by Eq. (4). (b) Bethe-Salpeter equation for the renormalized vertex functions $\Pi_\eta^{ss'}$. For the definition of diagram elements, see Fig. 2. We use the abbreviation $\bar{s} = -s$.

expression derived by Frigeri *et al.* [16] in the clean case. It also reproduces the results of Ref. [12], where the linearized gap equation was solved numerically in the disorder-free case, using a complex multiband model.

The result can be understood as follows. The effective magnetic field in the two valleys is given by $\mathbf{h}_\eta^{\mathrm{eff}} = h\mathbf{e}_x + \eta\Delta_{so}\mathbf{e}_z$, where $\mathbf{e}_i$ is a unit vector in the i direction. Electrons that are both aligned or antialigned with their respective "local" field have the same energy when their momenta are opposite and, thus, their contribution to pairing is not affected by the field. As at finite h the local fields are not along the same axis; however, they enter the gap equation with a suppressed weight $\Delta_{so}^2/(h^2 + \Delta_{so}^2)$, determined by the overlap of their spin directions. If one electron is aligned whereas the other electron is antialigned with their respective local field, they have an energy difference of $2\sqrt{h^2 + \Delta_{so}^2}$ when their momenta are opposite and, thus, their contribution to pairing is suppressed by the field. Here the weight is given as $h^2/(h^2 + \Delta_{so}^2)$, which is what appears in Eq. (8). Since intravalley scattering does not allow for spin flips, it does not change the result.

As seen in Fig. 4, h_{c2} is enhanced in the presence of spin-orbit coupling, especially at low temperatures. In fact, it diverges in the zero-temperature limit for finite Δ_{so}. Physically, this can be understood as a consequence of the inability of the Zeeman field to completely align the electron spins in the in-plane orientation, due to the antiparallel out-of-plane field provided by the Ising SOC.

For weak Ising SOC ($\Delta_{so} \ll \Delta_0$), the critical curve $h_{c2}(T)$ significantly deviates from the conventional one only at very low temperature, where it diverges (in logarithmic accuracy) as

$$h_{c2} \propto \Delta_{so}\sqrt{\ln\frac{T_c}{T}} \quad \text{for} \quad \frac{T}{T_c} \ll \exp\left(-c\frac{\Delta_0^2}{\Delta_{so}^2}\right), \qquad (9)$$

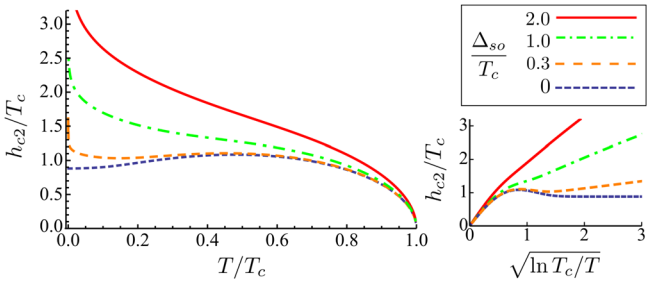

FIG. 4. Upper critical field as a function of temperature in the absence of intervalley scattering for different values of Ising SOC, as described by Eq. (8). The plot on the right shows the same result but with a different scale for the x axis to illustrate the logarithmic divergence at low temperature when $\Delta_{so} \neq 0$.

where c is a constant of order 1. Close to T_c, one obtains the standard result $h_{c2} \approx 2.16 T_c \sqrt{1 - T/T_c}$.

In the more interesting case of large Ising SOC, $\Delta_{so} \gg \Delta_0$, Eq. (8) yields a logarithmic divergence starting at higher temperatures,

$$h_{c2} \approx \Delta_{so} \sqrt{\ln \frac{T_c}{T} / \ln \frac{2\Delta_{so}}{\Delta_0}} \quad \text{for} \quad \frac{T}{T_c} \ll \frac{\Delta_0}{\Delta_{so}}. \tag{10}$$

Close to T_c, the critical field exhibits a standard square-root dependence on temperature, but with an enhanced prefactor,

$$h_{c2} \approx \Delta_{so} \frac{1}{\sqrt{\ln \frac{2\Delta_{so}}{\Delta_0}}} \sqrt{1 - \frac{T}{T_c}}. \tag{11}$$

With intervalley scattering.—At finite magnetic field, intervalley scattering provides an effective spin-flip mechanism, since electrons scattered between two valleys "feel" opposite values of the Ising SOC field. This pair-breaking effect leads to a saturation of h_{c2} at zero temperature, as illustrated in Fig. 5. For weak intervalley disorder, $1/\tau_2 \ll \Delta_0 \ll \Delta_{so}$, we estimate the zero-temperature critical field as

$$h_{c2} \approx \Delta_{so} \sqrt{\ln(\Delta_0 \tau_2) / \ln \frac{2\Delta_{so}}{\Delta_0}} \tag{12}$$

in logarithmic accuracy. In the vicinity of T_c, the critical line is still described by Eq. (11) in that parameter regime.

On the other hand, the standard expression for the second-order paramagnetically limited critical line, given by Eq. (8) at $\Delta_{so} = 0$, is recovered at large disorder strength, $1/\tau_2 \gg \Delta_{so}^2/\Delta_0$. In this regime, electrons are frequently scattered between two valleys and do not "feel" the effect of valley-dependent Ising SOC anymore.

Nature of the transition.—In the absence of SOC, the phase transition is a second-order transition into a uniform superconducting state only at sufficiently high temperature. A nonuniform (Fulde-Ferrell-Larkin-Ovchinnikov, or FFLO) phase could possibly contribute to the enhancement of h_{c2}, as it was recently discussed in clean bilayer TMDC superconductors [31]. In order to study the nature of the transition in the clean case, we generalize the expression for the gap equation (4) by adding quadratic corrections in a finite modulation wave vector and cubic corrections in the gap amplitude Δ [30]. We find that both do not affect the transition when $\Delta_{so} \gtrsim \Delta_0$. Moderate disorder is not expected to change these conclusions [32].

Discussion and conclusion.—Experiments [12,13,15] revealed superconductivity in TMDC well above the Pauli limit. The measured fields remained, however, below the values expected in the clean case with Ising SOC only. In Ref. [12], Rashba SOC was considered as a possible mechanism for the suppression of h_{c2} at low temperature. However, the model required an irrealistically large amplitude for the Rashba SOC. Our work shows that moderate intervalley scattering, which has already been invoked in Ref. [24] in the normal state, could provide an alternative scenario for the saturation. The curve corresponding to $1/(\tau_2 T_c) = 1.5$ shown in Fig. 5(c) gives a good fit of the

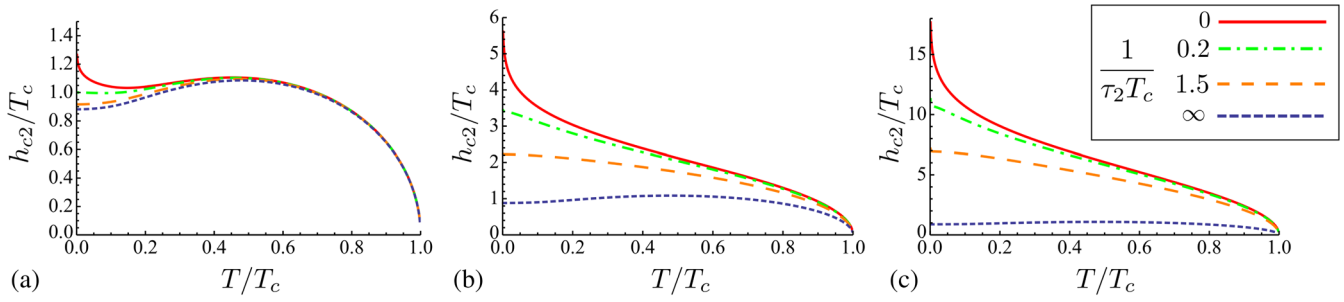

FIG. 5. Upper critical field as a function of the temperature for various strengths of Ising SOC and intervalley scattering: (a) $\Delta_{so}/T_c = 0.3$, (b) $\Delta_{so}/T_c = 3$, and (c) $\Delta_{so}/T_c = 12$. The choice of parameters $\Delta_{so}/T_c = 12$ and $1/(\tau_2 T_c) = 1.5$ [dashed line in (c)] gives a good fit of the experimental data from Ref. [12] taking the g factor to be $g = 2$.

experimental data from Ref. [12] using their estimate for Δ_{so}/T_c.

In conclusion, we have studied the effect of disorder on TMDC monolayer superconductors. We have predicted that the large enhancement of the upper critical magnetic field is robust to intravalley scattering. Furthermore, we have identified intervalley scattering as a likely mechanism for the more moderate enhancement of h_{c2} observed in experiment. Interestingly, TMDCs have been identified as a possible platform for topological superconductivity and Majorana fermions [33] provided that unconventional pairing takes place. The role of disorder within these scenarios can be investigated within the theory frame provided by our work.

We acknowledge funding from the Laboratoire d'excellence LANEF in Grenoble (ANR-10-LABX-51-01) and by the ANR through Grant No. ANR-16-CE30-0019.

[1] Q. H. Wang, K. Kalantar-Zadeh, A. Kis, J. N. Coleman, and M. S. Strano, Nat. Nanotechnol. **7**, 699 (2012).
[2] K. F. Mak and J. Shan, Nat. Photonics **10**, 216 (2016).
[3] K. F. Mak, C. Lee, J. Hone, J. Shan, and T. F. Heinz, Phys. Rev. Lett. **105**, 136805 (2010).
[4] B. Radisavljevic, A. Radenovic, J. Brivio, I. V. Giacometti, and A. Kis, Nat. Nanotechnol. **6**, 147 (2011).
[5] B. T. Zhou, N. F. Q. Yuan, H.-L. Jiang, and K. T. Law, Phys. Rev. B **93**, 180501 (2016).
[6] Z. Zhu, Y. Cheng, and U. Schwingenschlögl, Phys. Rev. B **84**, 153402 (2011).
[7] A. Kormányos, G. Burkard, M. Gmitra, J. Fabian, V. Zólyomi, N. D. Drummond, and V. Fal'ko, 2D Mater. **2**, 022001 (2015).
[8] D. Xiao, G.-B. Liu, W. Feng, X. Xu, and W. Yao, Phys. Rev. Lett. **108**, 196802 (2012).
[9] K. F. Mak, K. He, J. Shan, and T. F. Heinz, Nat. Nanotechnol. **7**, 494 (2012).
[10] H. Zeng, J. Dai, W. Yao, D. Xiao, and X. Cui, Nat. Nanotechnol. **7**, 490 (2012).
[11] Q. H. Wang, K. Kalantar-Zadeh, A. Kis, J. N. Coleman, and M. S. Strano, Nat. Nanotechnol. **7**, 699 (2012).
[12] Y. Saito, Y. Nakamura, M. S. Bahramy, Y. Kohama, J. Ye, Y. Kasahara, Y. Nakagawa, M. Onga, M. Tokunaga, T. Nojima *et al.*, Nat. Phys. **12**, 144 (2016).
[13] J. Lu, O. Zheliuk, I. Leermakers, N. F. Yuan, U. Zeitler, K. T. Law, and J. Ye, Science **350**, 1353 (2015).
[14] M. Tinkham, *Introduction to Superconductivity* (Courier Corporation, Mineola, New York, 1996).
[15] X. Xi, Z. Wang, W. Zhao, J.-H. Park, K. T. Law, H. Berger, L. Forró, J. Shan, and K. F. Mak, Nat. Phys. **12**, 139 (2016).
[16] P. A. Frigeri, D. F. Agterberg, A. Koga, and M. Sigrist, Phys. Rev. Lett. **92**, 097001 (2004).
[17] K. Maki, Phys. Rev. **148**, 362 (1966).
[18] R. A. Klemm, A. Luther, and M. Beasley, Phys. Rev. B **12**, 877 (1975).
[19] V. Barzykin and L. P. Gor'kov, Phys. Rev. Lett. **89**, 227002 (2002).
[20] N. Reyren, S. Gariglio, A. Caviglia, D. Jaccard, T. Schneider, and J.-M. Triscone, Appl. Phys. Lett. **94**, 112506 (2009).
[21] T. Sekihara, R. Masutomi, and T. Okamoto, Phys. Rev. Lett. **111**, 057005 (2013).
[22] V. M. Edelstein, Sov. Phys. JETP **68**, 1244 (1989).
[23] A. K. Geim and I. V. Grigorieva, Nature (London) **499**, 419 (2013).
[24] H. Schmidt, I. Yudhistira, L. Chu, A. H. Castro Neto, B. Özyilmaz, S. Adam, and G. Eda, Phys. Rev. Lett. **116**, 046803 (2016).
[25] Similar considerations in graphene, where $\Delta_B = \Delta_A$ and $E_g = 0$, lead to the suppression of Ising SOC in the projected basis.
[26] Ref. [27] analyzes the effect of disorder when μ lies in the vicinity of E_g and only one spin-band per cone is occupied.
[27] E. Sosenko, J. Zhang, and V. Aji, Phys. Rev. B **95**, 144508 (2017).
[28] I. L. Aleiner and K. B. Efetov, Phys. Rev. Lett. **97**, 236801 (2006).
[29] A. Altland, Phys. Rev. Lett. **97**, 236802 (2006).
[30] See the Supplemental Material at http://link.aps.org/supplemental/10.1103/PhysRevLett.119.117001 which contains technical details of the derivation of Eq. (7), its analysis in the limits $T \to 0$ and $T \to T_c$, and considerations about a possible transition into a nonuniform (FFLO) phase and/or a change of the order of the transition.
[31] C. X. Liu, Phys. Rev. Lett. **118**, 087001 (2017).
[32] As at large enough intervalley scattering Ising SOC becomes irrelevant, we expect to recover the standard first-order transition at low temperatures in this regime.
[33] N. F. Q. Yuan, K. F. Mak, and K. T. Law, Phys. Rev. Lett. **113**, 097001 (2014).